Electronic Supplementary Material (ESI) for Journal of Materials Chemistry A.


# *In situ* TEM investigation of large crystals formation in lithiated SnO2 anode assisted by electron beam irradiation

Yifeng Wen[a,#], Mingyun Zhu[a,#], Shugui Song[a], Lei Xin[a], Yuwei Xiong[a], Jingcang Li[a], Yuting Shen[b], Kuibo Yin*[a], Litao Sun*[a]

[a] SEU-FEI Nano-Pico Center, Key Laboratory of MEMS of Ministry of Education, Southeast University, Nanjing, 210096, P. R. China

[b] School of Electronic and Information Engineering, Changshu Institute of Technology, Changshu, 215500, P. R. China

#These authors contributed equally to this work.

* Corresponding authors.

E-mail addresses: yinkuibo@seu.edu.cn (K. Yin), and slt@seu.edu.cn (L. Sun)

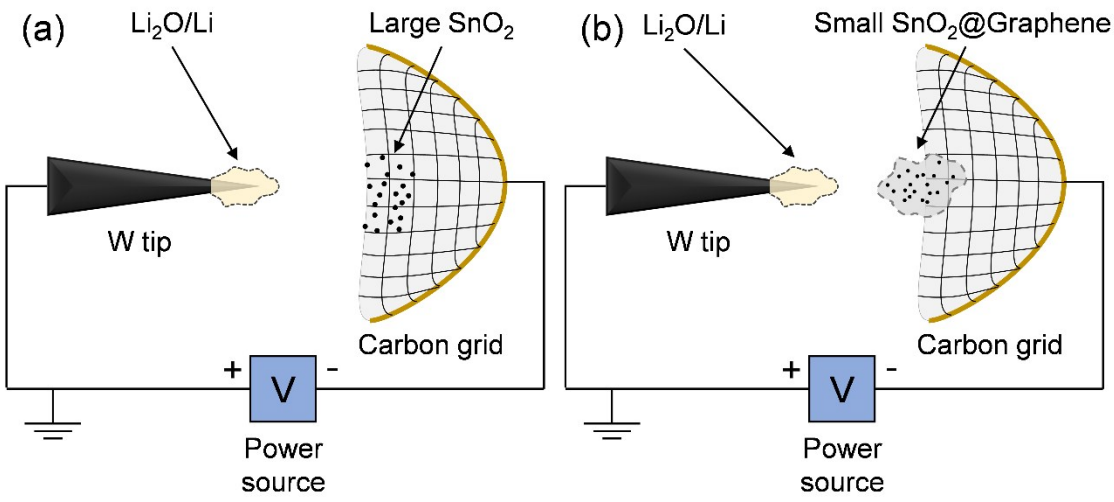


Fig S1. Schematic illustration of the experimental setup for (a) large $SnO_2$ sample (larger than 50 nm) and (b) small $SnO_2$ sample (smaller than 50 nm).

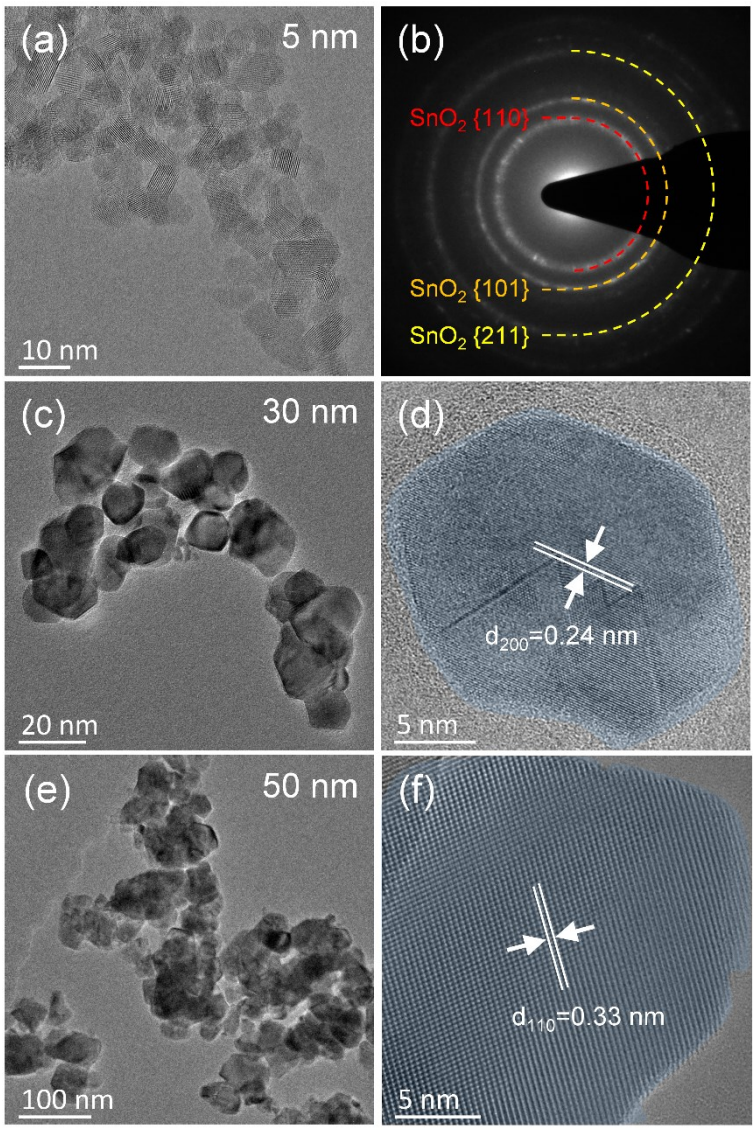


Fig S2. $SnO_2$ nanoparticles with different size (a, b) 5 nm; (c, d) 30 nm; (e, f) 50 nm.

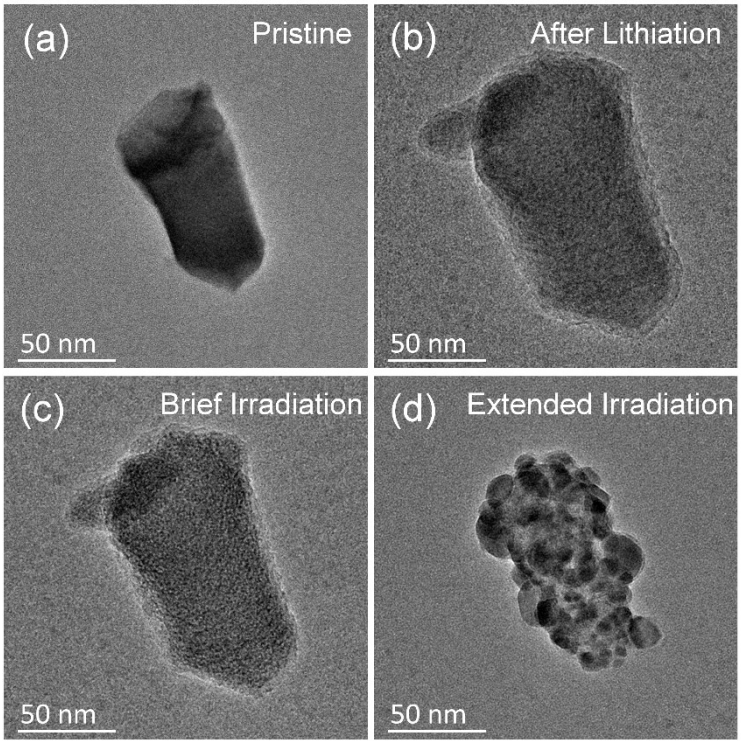


Fig S3. The structural transformation of a $SnO_2$ particles after lithiation and after irradiation. The pristine crystalline $SnO_2$ particle (a) was converted to the amorphous phase after lithiation (b). The sample was then be irradiated by electron beam with the lithium source removed. After brief irradiation (c), the amorphous sample shrank, and SEI decomposed. With the irradiation extending (d), numerous large crystals were formed.

**Facets Matching Method**

For each 2D lattice image, two sets of lattices, $d_{1exp}$ and $d_{2exp}$ and the crossing angle $\theta_{exp}$ can be directly measured from the image. In order to check if the certain phase might expose a similar 2D lattice, the following comparison algorithm is applied.

1. Calculate theoretical lattice spacing for each facet. The theoretical interplanar spacing $d_{theo}$ of *(h, k, l)* plane with crystal constant *(a, b, c, α, β, γ)* is calculated according to Eq. 1:

$$d_{theo}^2=V^2/((S_{11}h)^2 + (S_{22}k)^2 + (S_{33}l)^2 + 2(S_{12}hk + S_{13}hl + S_{23}kl)) \quad \text{(Eq.1)}$$

where $V=abc(1-\cos(\alpha)^2-\cos(\beta)^2-\cos(\gamma)^2+2\cos(\alpha)\cos(\beta)\cos(\gamma))$, $S_{11}=bc\sin(\alpha)$, $S_{22}=ac\sin(\beta)$, $S_{33}=ab\sin(\gamma)$, $S_{12}=abc^2(\cos(\alpha)\cos(\beta)-\cos(\gamma))$, $S_{13}=ab^2c(\cos(\alpha)\cos(\gamma)-\cos(\beta))$, $S_{23}=a^2bc(\cos(\beta)\cos(\gamma)-\cos(\alpha))$.

2. Create comparison list. The comparison list $D_{d1exp}$[n] and $D_{d2exp}$[m] of the experimentally observed lattice spacing is secondly created. If abs($d_{theo}$ - $d_{exp}$) < $\delta d$, where $\delta d$ is the pre-defined accuracy, vector *(h, k, l, $d_{theo}$)* will be appended to the $D_{dexp}$[n].

3. Calculate theoretical crossing angle. After obtaining both the $D_{d1exp}$[n] and $D_{d2exp}$[m], the theoretical crossing angle $\theta_{theo}$[i, j] between $D_{d1exp}$[i], i∈n, and $D_{d2exp}$[j], j∈m, is calculated according to Eq. 2:

$$\theta_{theo}[i, j] = d_{1theo}[i]\ d_{2theo}[j]/(V^2(S_{11}h_1[i]h_2[j]+S_{22}k_1[i]k_2[j]+ S_{33}l_1[i]l_2[j]+ S_{12}h_1[i]k_2[j]+S_{12}k_1[i]h_2[j]+S_{13}h_1[i]l_2[j]+S_{13}l_1[i]h_2[j]+S_{23}k_1[i]l_2[j]+S_{23}l_1[i]h_2[j])) \quad \text{(Eq.2)}$$

If the theoretical crossing angle is within the permittable error range to the experimental angle, namely abs($\theta_{theo}$[i, j] -$\theta_{exp}$ ) < $\delta\theta$, ($h_1$, $k_1$, $l_1$) and ($h_2$, $k_2$, $l_2$) are considered as a set of matching 2D lattice. In this paper, $\delta d$ is set to 0.05Å and $\delta\theta$ set to 3°.

**Table S1. Matching results for the three facets in Figure 2.**

| Phase \ Lattice | $d_{1exp}$=0.28nm, $d_{2exp}$=0.28nm, $\theta_{exp}$=139° | $d_{1exp}$=0.28nm, $d_{2exp}$=0.20nm, $\theta_{exp}$=78° | $d_{1exp}$=0.29nm, $d_{2exp}$=0.28nm, $\theta_{exp}$=90° |
|---|---|---|---|
| Tetragonal Sn | No Match | $d_{101}$=0.279nm, $d_{-211}$=0.201nm, $\theta_{theo}$=77.0° | $d_{200}$=0.291nm, $d_{011}$=0.279nm, $\theta_{theo}$=90.0° |
| Cubic Sn | No Match | No Match | No Match |
| LiSn | No Match | No Match | No Match |
| $Li_5Sn_2$ | No Match | $d_{10\text{-}5}$=0.285nm, $d_{022}$=0.201nm, $\theta_{theo}$=78.8° | No Match |
| $Li_7Sn_3$ | No Match | $d_{2\text{-}21}$=0.285nm, $d_{-122}$=0.206nm, $\theta_{theo}$=80.4° | No Match |
| $Li_7Sn_2$ | No Match | $d_{240}$=0.282nm, $d_{4\text{-}21}$=0.208nm, $\theta_{theo}$=76.0° | No Match |
| $Li_{13}Sn_5$ | No Match | $d_{007}$=0.283nm, $d_{022}$=0.201nm, $\theta_{theo}$=78.0° | No Match |
| $Li_{22}Sn_5$ | $d_{-107}$=0.279nm, $d_{34\text{-}5}$=0.279nm, $\theta_{theo}$=139.5° | $d_{700}$=0.283nm, $d_{29\text{-}3}$=0.204nm, $\theta_{theo}$=78.1° | $d_{603}$=0.295nm, $d_{700}$=0.283nm, $\theta_{theo}$=90.0° |

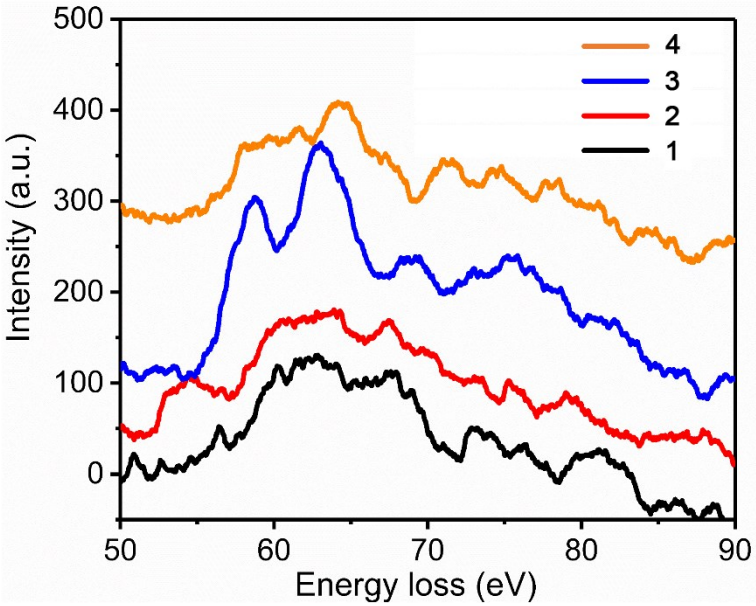


Fig S4. EELS spectra of the Li-K edge of the carbon support with different treatments: (1) 30 mins' placement with 0 min's irradiation; (2) 30 mins' placement with 15 mins' irradiation; (3) 0 min's placement with 0 min's irradiation; (4) 0 min's placement with 25 mins' irradiation.

The spectra were collected in the same carbon support area (~150 nm apart from the sample) under an imaging mode. For spectrum 1 (black line), it was collected when the freshly lithiated $SnO_2$ particle (~70 nm) was placed for 30 min. Subsequently, the entire area with a diameter about 1 μm, including the employed carbon area and the lithiated $SnO_2$, was irradiated under an electron beam dose of $1.19\times10^5$ A $m^{-2}$. When the irradiation time reached to 15 minutes, the EELS spectrum was then collected in the carbon support area (red line, 2). After that, the $SnO_2$ sample was re-lithiated and the EELS spectrum was immediately acquired without placement and irradiation (blue line, 3). Finally, the entire area was irradiated for 25 minutes and the EELS spectrum was obtained (orange line, 4).

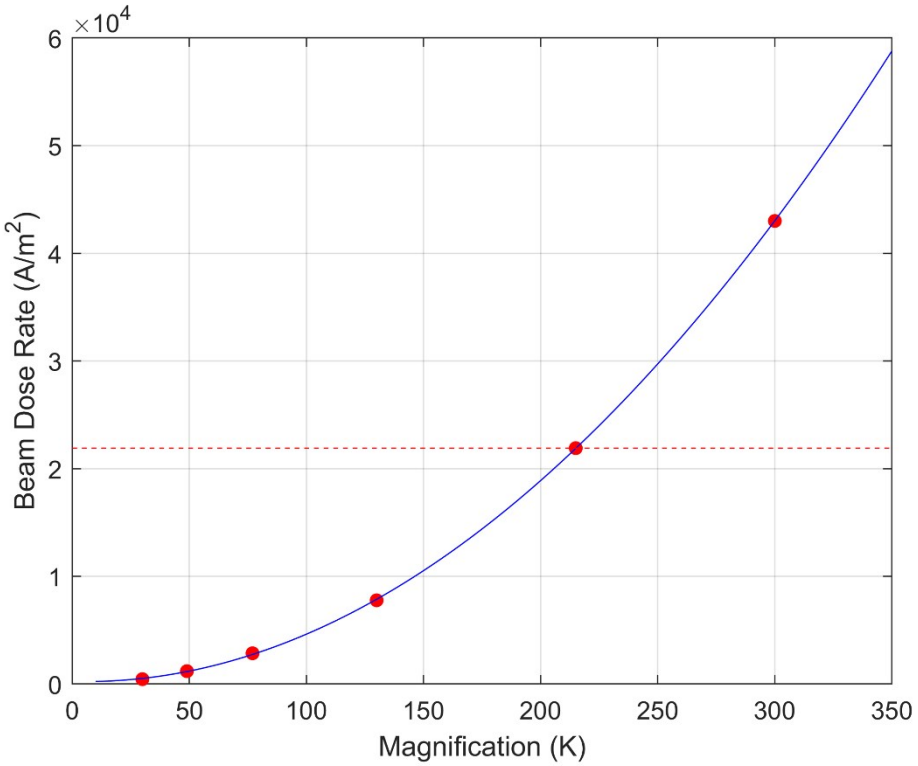


Fig S5. The quadric dependency between the Beam Dose Rate and TEM Magnification. Electron beam with dose rate beyond 21940 A $m^{-2}$ can result in large crystal formation in a lithiated $SnO_2$ particle.

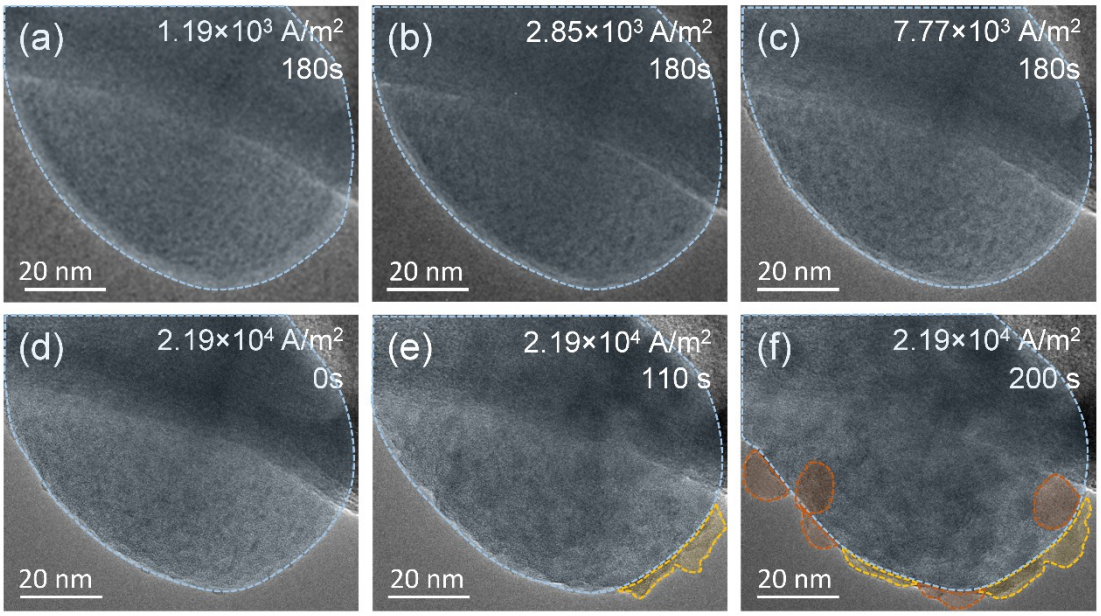


Figure S6. The effect of electron beam irradiation on the amorphous lithiated $SnO_2$ particle. The amorphous particle was irradiated by an electron beam for 180 s under a sequentially increasing dose rate of (a) 1190 A $m^{-2}$, (b) 2850 A $m^{-2}$, (c) 7770 A $m^{-2}$, and (d-f) 21900 A $m^{-2}$. The formation of large crystal (marked in orange) was observed after the amorphous sample being irradiated for 200 s under the dose rate of 21900 A $m^{-2}$.

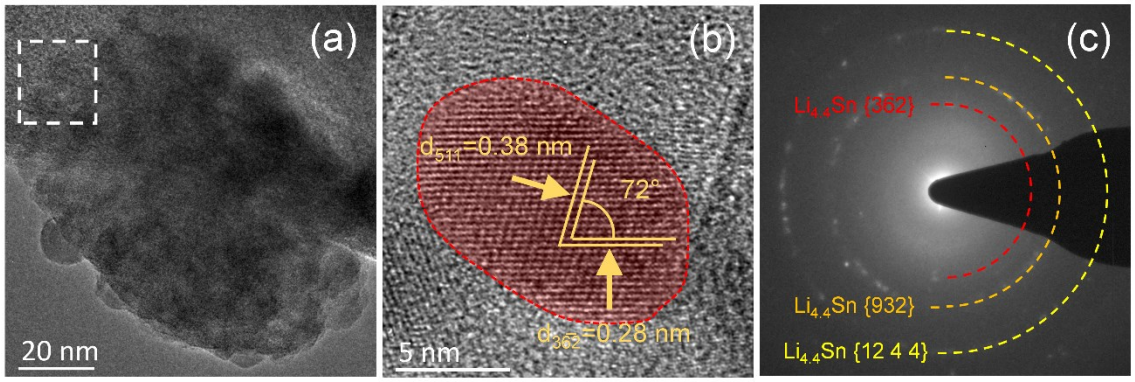


Figure S7. Identification of the phase of formed large crystal in the irradiated sample. (a) TEM image of the sample after 200s' irradiation at $2.19\times10^4$ A $m^{-2}$. (b) HRTEM of one nanocrystal. (c) SAED image of the sample.

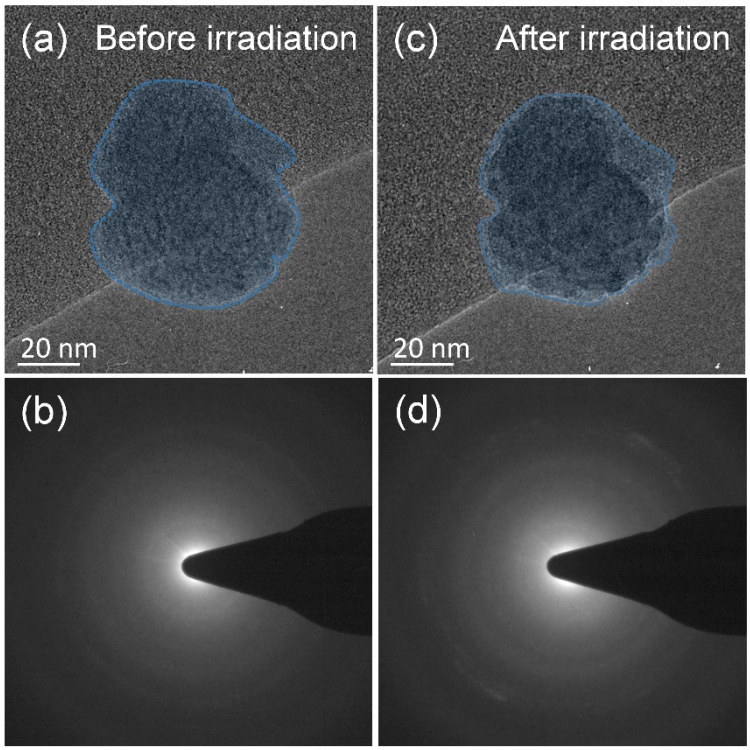


Fig S8. Extending irradiation experiment of lithiated $SnO_2$ particle with a moderate dose rate. (a, b) TEM and SAED image of the amorphous sample before irradiation. (c, d) TEM and SAED image of the sample after irradiation. Beam dose: $6.13\times10^3$ A $m^{-2}$, Duration: 30 mins.

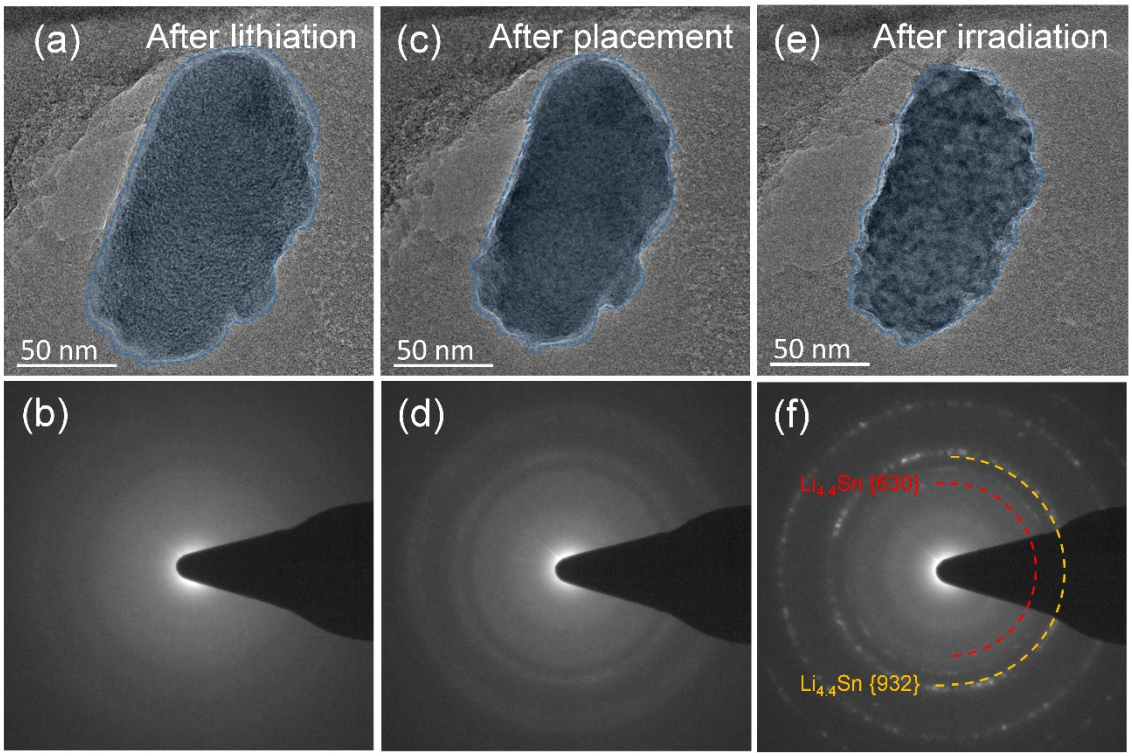


Fig S9. Phase transition of lithiated $SnO_2$ particle after placement and after irradiation. TEM and SAED image of the (a, b) freshly lithiated amorphous sample, (c, d) amorphous sample after placement, and (e, f) nanocrystalline sample after irradiation.

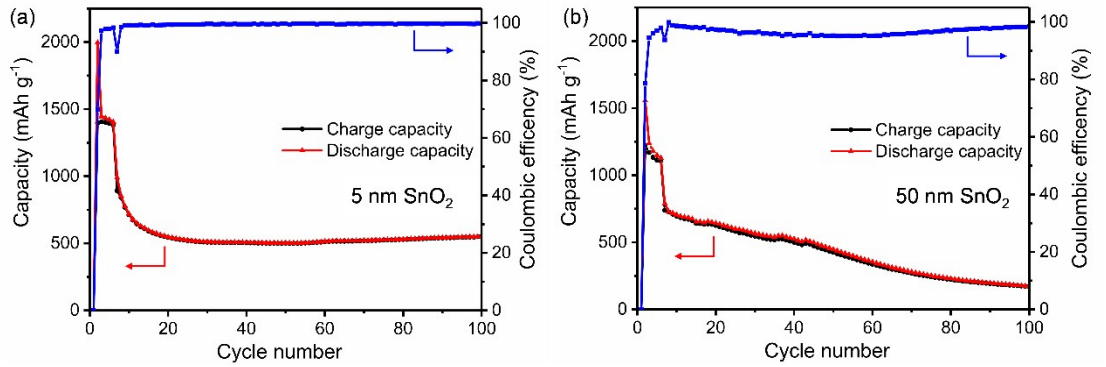


Figure S10. The cycling performance of (a) 5 nm $SnO_2$ and (b) 50 nm $SnO_2$ under a current density of 1000 mA $g^{-1}$ between the voltage range of 0.01 V and 3 V vs $Li^+/Li$. The cell was first discharged/charged under a small current density of 50 mA $g^{-1}$ during the initial 5 cycles to activate the anode materials. The small-sized $SnO_2$ showed superior cycling stability and reversibility compared with large $SnO_2$.

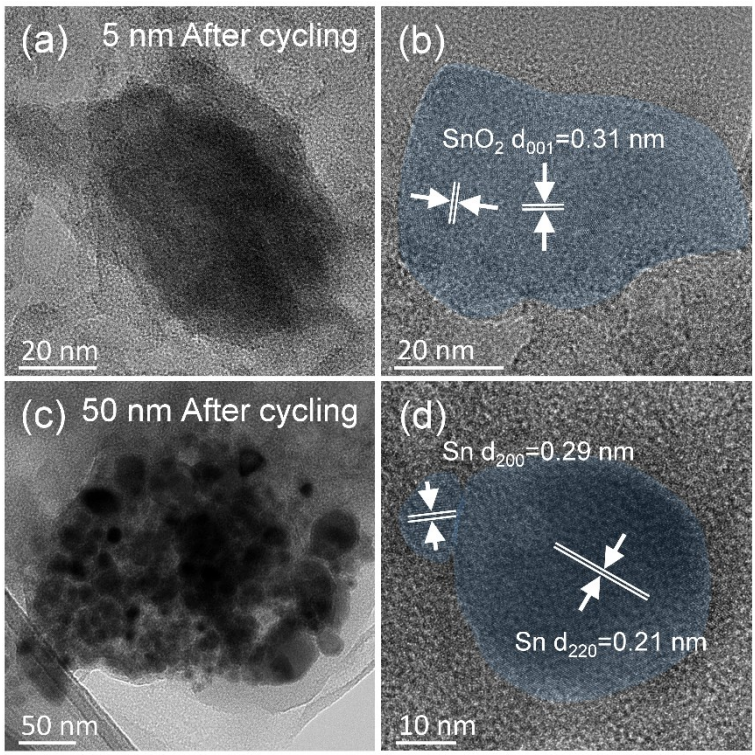


Fig S11. TEM and HRTEM images of the cycled anode in charged state. (a, b) 5 nm $SnO_2$ anode; (c, d) 50 nm $SnO_2$ anode.

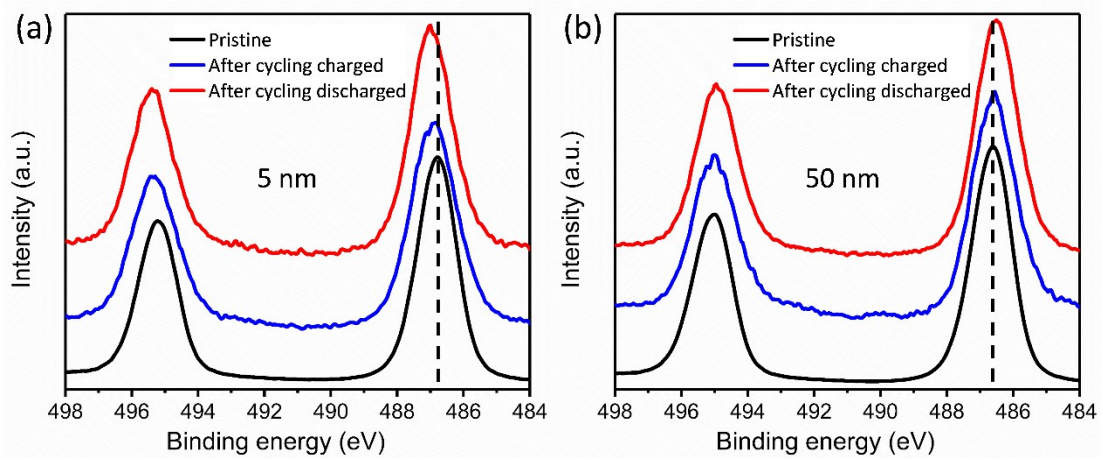


Fig S12. Sn 3d XPS spectra for the $SnO_2$ anode. (a) The pristine 5 nm $SnO_2$ anode, 5 nm $SnO_2$ anode after 100 cycles in charged and discharged state; (b) The pristine 50 nm $SnO_2$ anode, 50 nm $SnO_2$.